Journal of Materials Science: Materials in Electronics (2019) 30:5917–5922
https://doi.org/10.1007/s10854-019-00890-4

Structural evolution, dielectric and ferroelectric properties of (1-*x*) $Bi_{0.5}Na_{0.5}TiO_3$-*x*$Ba_{0.3}Sr_{0.7}TiO_3$ ceramics

Dongxu Li[1] · Zong-Yang Shen[1] · Zhipeng Li[1] · Xingcai Wang[2] · Wen-Qin Luo[1] · Fusheng Song[1] · Zhumei Wang[1] · Yueming Li[1]

Received: 23 January 2019 / Accepted: 4 February 2019 / Published online: 12 February 2019

Abstract

$(1-x)Bi_{0.5}Na_{0.5}TiO_3-xBa_{0.3}Sr_{0.7}TiO_3$ (abbreviated as BNT-BST, $x=0.05\sim0.40$) was prepared by a conventional ceramic processing method and their structural evolution, dielectric and ferroelectric properties were investigated. The structure of the BNT-BST ceramics changes from phase coexistences of Rhombohedral-Tetragonal ($x\leq0.10$) to Tetragonal-Cubic ($x\geq0.35$), across a dominant Tetragonal phase region ($0.15\leq x\leq0.30$). By increasing BST content, the grain size of the BNT-BST ceramics slightly decreases, while the temperature T_m of the maximum dielectric constant gradually goes downward from ~250 °C to near room temperature. Meanwhile, with the increase of measuring frequency, the T_m increases for the BNT-BST ceramics with $x\geq0.15$, indicating their relaxor ferroelectric characteristics. Room temperature *P-E* loop test results show that both coercive field E_c and remnant polarization P_r gradually reduce with the increase of x value for relaxor BNT-BST ceramics. Both high peak dielectric constant ($\varepsilon_r>6000$ at T_m) and saturated polarization ($P_s\sim30$ μC/cm^2), as well as tunable remnant polarization P_r are obtained in relaxor BNT-BST ceramics suitable for capacitor candidate materials.

1 Introduction

Ceramic capacitors are indispensable components in modern electronics, which are employed for functions of bypassing, coupling, decoupling, filtering, pulse discharge, power conditioning, and so on [1]. Ferroelectrics used for ceramic capacitors must satisfy many requirements in order to be used reliably in such applications. A high relative dielectric constant ε_r is essential for large valued capacitors with good volumetric efficiency and thus affords system miniaturization [2]. In general, normal ferroelectrics have very high ε_r in the vicinity of Curie temperature. However, such high ε_r in the vicinity of Curie temperature is not suitable for practical usage for capacitors due to its poor temperature dependence [3]. An effective method for improving temperature dependence of dielectric properties is to make the Curie peak diffuse and form so-called relaxor ferroelectrics [4]. During the past decades, lead-based relaxor ferroelectrics, typically represented by $Pb(Nb,Mg)O_3$–$PbTiO_3$ (PMN-PT), have been extensively studied and successfully commercialized [5–7]. However, lead-based ceramics will be prohibited in the future with increasing attention to environmental issues and human health. Therefore, it is desirable to develop lead-free ferroelectric ceramics with excellent dielectric properties for replacing the lead-containing ceramics in capacitor applications [8].

$Bi_{0.5}Na_{0.5}TiO_3$ (BNT), which is an environmentally friendly perovskite structural ferroelectric material with rhombohedral symmetry (*R*3*c*) at room temperature, has been attracted considerable attention due to its high promising dielectric and piezoelectric properties over a wide temperature range [9–11]. BNT exhibits extremely complex crystal structure and is characterized by temperature dependent permittivity with two anomalies at $T_d\sim200$ °C and $T_m\sim320$ °C [12, 13]. Previously, BNT was extensively studied as a promising lead-free piezoelectric candidate, because it can form a morphotropic phase boundary (MPB) with other tetragonal perovskites, such as $BaTiO_3$ (BT) and $Bi_{0.5}K_{0.5}TiO_3$ (BKT), and such MPB composition will show enhanced piezoelectric properties [14, 15]. However,

✉ Zong-Yang Shen
shenzongyang@163.com

[1] Energy Storage and Conversion Ceramic Materials Engineering Laboratory of Jiangxi Province, National Light Industry Key Laboratory of Functional Ceramic Materials, School of Materials Science and Engineering, Jingdezhen Ceramic Institute, Jingdezhen 333403, China

[2] Chengdu Hongming UESTC Electronic New Materials Co., Ltd, Chengdu 610100, China

the research of BNT as capacitor ceramic applications is far less extensive than that of BNT as piezoelectric ceramics because of its relatively low permittivity at room temperature ($\varepsilon_r \sim 760$ at 1 kHz). Recently, with the aim of improving room temperature permittivity and temperature dependent behavior, different compounds such as (Na,Bi)NbO_3 and $SrTiO_3$ modified BNT-based ceramics were investigated for energy storage capacitor applications [16, 17]. Moreover, some works about the application of BNT-based ceramics as high temperature capacitors have also been reported, because BNT can actually obtain good temperature dependent dielectric characteristics at elevated temperatures even up to 400 °C by modification [11, 18–20].

In our previous work, $Ba_{0.3}Sr_{0.7}TiO_3$ (BST) was found to be more suitable for preparation of pulse power capacitors [21, 22]. However, the room temperature permittivity ($\varepsilon_r \sim 650$ at 1 kHz) of BST is also relatively low due to its Curie temperature ($T_c = -85$ °C) far below room temperature. Consequently, in this work, a $(1-x)Bi_{0.5}Na_{0.5}TiO_3-xBa_{0.3}Sr_{0.7}TiO_3$ (BNT-BST) binary solid solution is developed to improve room temperature dielectric properties by designing to form relaxor ferroelectrics. Accordingly, the influence of BST content on the crystal structure, microstructure, dielectric and ferroelectric properties of the ceramics was comprehensively investigated.

2 Experimental procedures

A conventional processing method was applied to fabricate $(1-x)Bi_{0.5}Na_{0.5}TiO_3-xBa_{0.3}Sr_{0.7}TiO_3$ (BNT-BST) ceramics, in which x equals 0.05, 0.10, 0.15, 0.20, 0.25, 0.30, 0.35, and 0.40 respectively, by using raw materials of bismuth oxide (Bi_2O_3, 99%), sodium carbonate (Na_2CO_3, 99.8%), barium carbonate ($BaCO_3$, 99%), strontium carbonate ($SrCO_3$, 99%), and titanium dioxide (TiO_2, 98%) from Sinopharm Chemical Reagent Co. Ltd., Shanghai, China. The raw powders were weighed according to the stoichiometric formula of each composition and milled in a polyethylene jar for 24 h in ethanol medium with ZrO_2 balls. After separating the balls, the mixed slurry were dried and calcined at 850 °C for 3 h and then milled again for 24 h. The calcined powders were granulated to be pressed into disks of 13 mm diameter and about 1 mm thick under 120 ± 10 MPa by adding polyvinyl alcohol solution (PVA, 5 wt%) as a binder. The disks were first preheated in air at 650 °C for 2 h to remove PVA binders, and then sintered at temperatures ranging from 1140 °C to 1260 °C for 2 h in air with a heating rate of 5 °C/min and finally furnace-cooled to ambient temperature.

An X-ray diffraction (XRD, D8-Advance, Bruker, Germany) technique with CuK_α radiation ($\lambda = 0.15406$ nm) was used to determine the phase structure of sintered BNT-BST ceramics. Data analysis was carried out by a Rietveld method using the GSAS program suite. The microstructure features of the polished and thermally-etched surfaces of the sintered ceramics were characterized by a scanning electron microscopy (SEM, JSM-6700F, JEOL, Japan). The sintered ceramic samples were polished to about 0.8 mm thick for dielectric measurements. Silver pastes were painted on both sides of the polished ceramic samples, and then fired to electrodes at 800 °C for 20 min. The temperature dependence of the dielectric constant ε_r and loss tanδ was determined using a precision impedance analyzer (HP4294A, Agilent) over a temperature range from room temperature to 400 °C, being connected to a computer controlled temperature chamber. The data at testing frequencies of 1 kHz, 10 kHz, 100 kHz and 1 MHz are collected. The polarization–electric field (P–E) hysteresis loops were examined at room temperature using a Radiant precision workstation (TRek model 609B) based on a standard Sawyer–Tower circuit at 10 Hz.

3 Results and discussion

Figure 1a shows the XRD patterns of the BNT-BST ceramics with different x values. It can be seen that all ceramics have a pure perovskite phase, and no secondary phases can be traced within the detection accuracy of XRD technique. The zoomed XRD patterns in the 2θ range of 38° ~ 42° and 45° ~ 48° are given in Fig. 1b, c, respectively. For the BNT-BST ceramics with $x \le 0.10$, two splitting (003)/(021) diffraction peaks around $2\theta = 40°$ and one (202) diffraction peak around $2\theta = 46.5°$ are detected, in accordance with the structural characteristics of rhombohedral BNT phase [23]. When $x \ge 0.15$, only one diffraction peak can be detected around $2\theta = 40°$, but two splitting diffraction peaks appear around $2\theta = 46.5°$, and these two peaks gradually merge together with the increase of x followed by a basically one peak at $x = 0.35$. This phenomenon indicates a dominant tetragonal phase for the BNT-BST ceramics with $0.15 \le x \le 0.30$, while the appearance of cubic phase when $x \ge 0.35$.

To understand the detailed crystal structure of the BNT-BST ceramics, Rietveld refinement was performed and the results are given in Table 1. The selected Rietveld refinement profiles of the BNT-BST ceramics with $x = 0.05$, 0.15, and 0.35 are shown in Fig. 2. The profile R-value (R_p), weighted profile R-value (R_{wp}) and χ^2-value of the refined structure parameters indicate that the refinement results are acceptable. As shown in Table 1, the phase structure evolution of the BNT-BST ceramics with increasing BST content can be clearly identified. The BNT-BST ceramics hold a coexistence of Rhombohedral ($R3c$) and Tetragonal ($P4bm$) phases when $x \le 0.10$, but a coexistence of Tetragonal ($P4bm$) and Cubic ($Pm\bar{3}m$) phases when $x \ge 0.35$, passing through a dominant Tetragonal ($P4bm$) phase region with $0.15 \le x \le 0.30$.

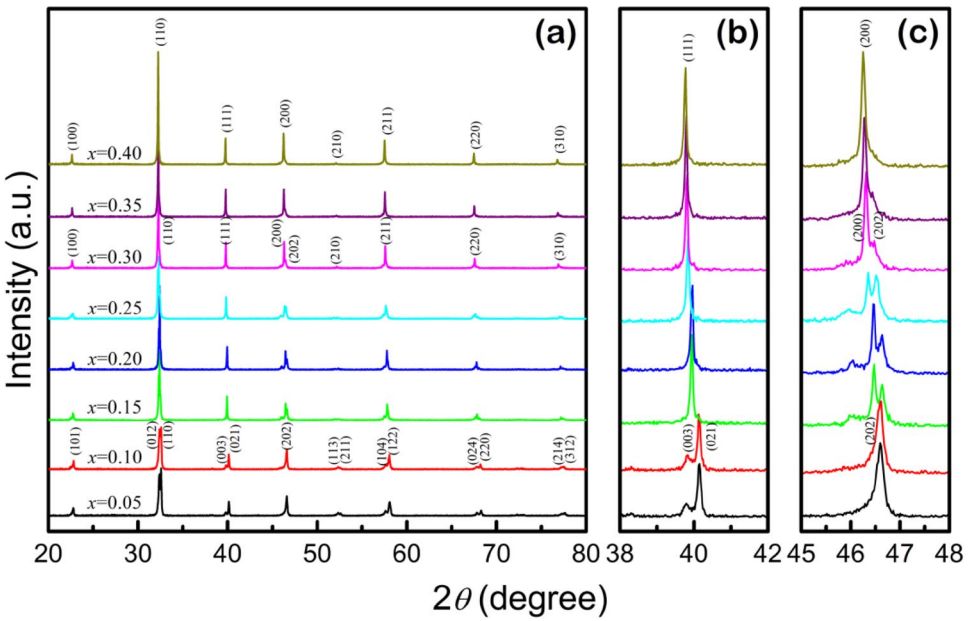

Fig. 1 XRD patterns of the BNT-BST ceramics in the ranges of 2θ **a** from 20°–80°, **b** from 38°–42°, and **c** from 45°–48°

Table 1 Rietveld refinement results of the BNT-BST ceramics with different x values

x	Phase	Lattice parameters		R_p (%)	R_{wp} (%)	χ^2
		a	c			
0.05	*R*3*c* 41.64%	5.4864	13.5594	5.61	8.07	2.051
	*P*4*bm* 58.36%	5.5464	3.9297			
0.10	*R*3*c* 38.76%	5.4973	13.5698	5.94	8.92	2.335
	*P*4*bm* 61.24%	5.5247	3.9398			
0.15	*P*4*bm*	5.5143	3.9295	6.23	9.62	2.577
0.20	*P*4*bm*	5.5192	3.9285	6.84	9.78	3.097
0.25	*P*4*bm*	5.5215	3.9390	6.11	9.29	2.392
0.30	*P*4*bm*	5.5224	3.9436	5.93	8.88	2.119
0.35	*P*4*bm* 69.63%	5.5301	3.9434	6.00	9.06	2.229
	$Pm\bar{3}m$ 30.37%	3.9197	3.9197			
0.40	*P*4*bm* 68.32%	5.5369	3.9417	5.92	9.09	2.193
	$Pm\bar{3}m$ 31.68%	3.9218	3.9218			

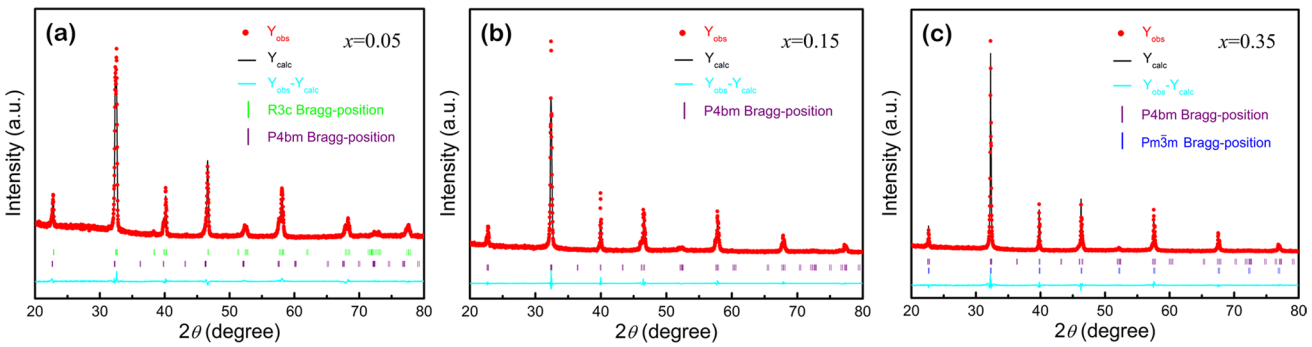

Fig. 2 Rietveld refinement profiles of the BNT-BST ceramics: **a** $x=0.05$; **b** $x=0.15$; and **c** $x=0.35$. Solid circles show the measured data points, and the solid line represents the calculated diffraction pattern

Figure 3 shows the microstructure features of the thermally-etched surfaces of the BNT-BST ceramics with different x values. It can be seen from Fig. 3 that all ceramics achieve high density with clear grains and grain boundaries. Basically, the grain size gradually decreases with the increase of BST content. For the BNT-BST ceramics with $x=0.05$ (see Fig. 3a), the gain size is up to 10 μm. However, the grain size can be reduced to ~2 μm for BNT-BST ceramics with $x=0.40$ (see Fig. 3h).

Figure 4 shows the temperature dependent dielectric constant and loss of the BNT-BST ceramics with different x values. It was reported that the temperature dependence of the dielectric permittivity of undoped BNT shows two anomalies: a broad maximum at T_m ~ 320 °C corresponding to a transition from a paraelectric to a presumed antiferroelectric (AFE) phase, and a shoulder hump at ~200 °C attributed to a transition to a ferroelectric state, which is often designated as a depolarization temperature T_d accompanied by a decay of spontaneous polarization [13, 24]. For the BNT-BST ceramics with $x \leq 0.10$, as shown in Fig. 4a, b, the temperature dependent dielectric constant exhibits similar behavior to that of undoped BNT, but the T_m and T_d are all decreased. For example, the T_m and T_d are observed to be ~230 °C and ~120 °C, respectively for the BNT-BST ceramics with $x=0.10$. However, only T_m can be observed for the BNT-BST ceramics with $x \geq 0.15$, as shown in Fig. 4c–h. Moreover, the temperature dependent dielectric constant behavior is satisfied with a generic feature of relaxor ferroelectrics: the T_m shifts to higher temperature as the frequency of the probing field increases [25]. In general, with the increase of BST content x, the T_m of the BNT-BST ceramics gradually shifts

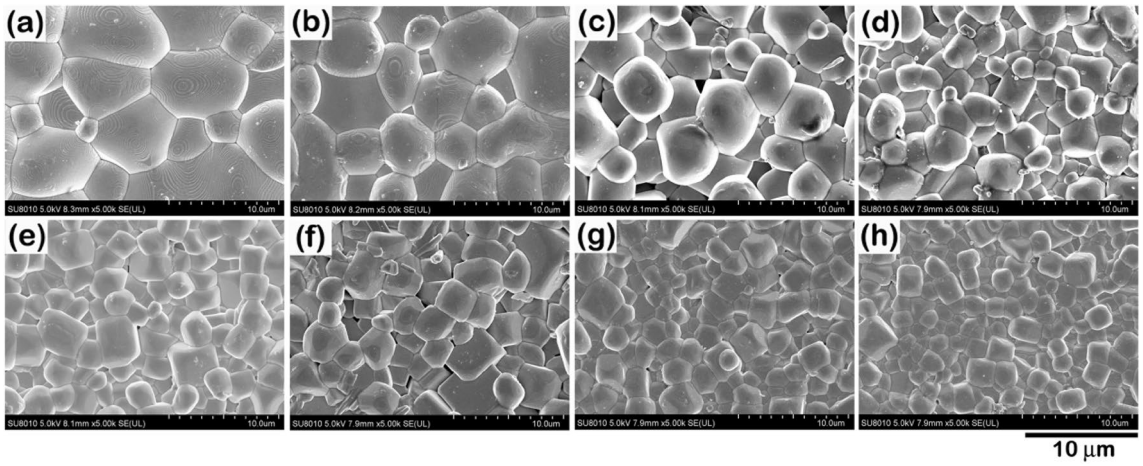

Fig. 3 SEM images of the polished and thermally-etched BNT-BST ceramics: **a** $x=0.05$; **b** $x=0.10$; **c** $x=0.15$; **d** $x=0.20$; **e** $x=0.25$; **f** $x=0.30$; **g** $x=0.35$; and **h** $x=0.40$

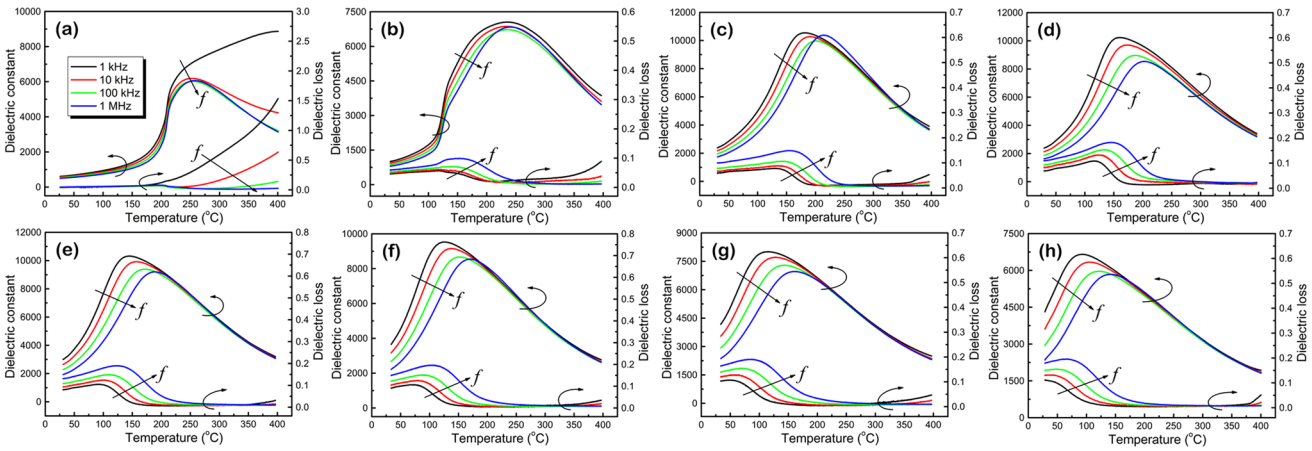

Fig. 4 Temperature dependent of dielectric constant and loss of the BNT-BST ceramics: **a** $x=0.05$; **b** $x=0.10$; **c** $x=0.15$; **d** $x=0.20$; **e** $x=0.25$; **f** $x=0.30$; **g** $x=0.35$; and **h** $x=0.40$

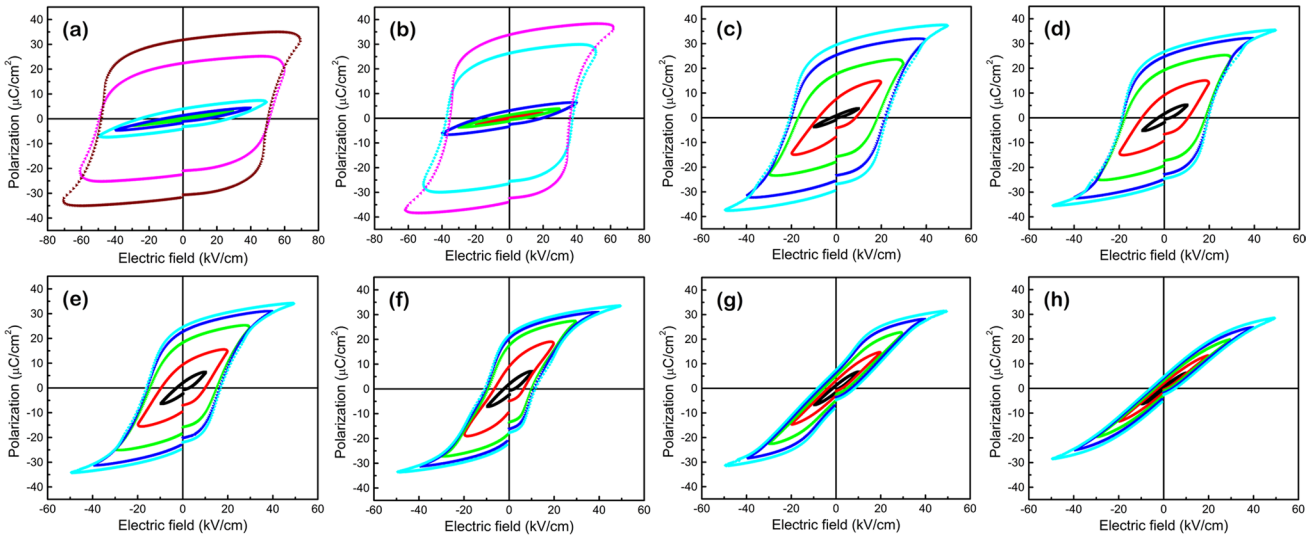

Fig. 5 Polarization–electric field (*P–E*) hysteresis loops of the BNT-BST ceramics: **a** $x=0.05$; **b** $x=0.10$; **c** $x=0.15$; **d** $x=0.20$; **e** $x=0.25$; **f** $x=0.30$; **g** $x=0.35$; and **h** $x=0.40$

downward to near room temperature. Therefore, the room temperature dielectric constant of the BNT-BST ceramics gradually increases with the BST content due to the relaxor ferroelectric characteristics of the ceramics and high peak dielectric constant ($\varepsilon_r > 6000$) at T_m. Actually, when BST content $x \geq 0.30$, the room temperature dielectric constant of the ceramics at 1 kHz is close to 4000 (see Fig. 4f), and even 4500 (see Fig. 4g, h), showing a very high level.

Figure 5 shows the room temperature *P-E* hysteresis loops of the BNT-BST ceramics with different x values measured at different applied electric fields until saturation. For BNT-BST ceramics with $x=0.05$ (see Fig. 5a), the loop displays a well-saturated ferroelectric behavior with both large remnant polarization ($P_r = 31.2$ μC/cm^2) and coercive field ($E_c = 50$ kV/cm) under an applied electric field of 70 kV/cm. When BST content is increased to $x=0.10$ (see Fig. 5b), a well-saturated loop is obtained under an applied electric field of 60 kV/cm accompanied by a little increased P_r (33.8 μC/cm^2) but apparently reduced E_c (35.6 kV/cm). With further increasing BST content ($x \geq 0.15$), both the P_r and E_c are gradually decreased, and the *P–E* loop even becomes slanted slim for BNT-BST ceramics with $x=0.40$ (see Fig. 5h), being marked with a low P_r (4.3 μC/cm^2) and sustained high P_s (~ 30 μC/cm^2). It is supposed that the ferroelectric order is disturbed with the increase of BST, leading to a ferroelectric to relaxor state transformation, as confirmed by the temperature dependent dielectric properties shown in Fig. 4. Therefore, the suppressed ferroelectricity of the BNT-BST ceramics is believed to be induced by an enhanced nonpolar tetragonal (*P*4*bm*) and/or Cubic ($Pm\bar{3}m$) structure with the increase of BST content as analyzed by XRD results (see Fig. 2; Table 1).

4 Conclusions

In summary, the structure of $(1-x)Bi_{0.5}Na_{0.5}TiO_3$–$xBa_{0.3}Sr_{0.7}TiO_3$ (BNT-BST) ceramics is revealed to be changing from phase coexistences of Rhombohedral-Tetragonal ($x \leq 0.10$) to Tetragonal-Cubic ($x \geq 0.35$), across a dominant Tetragonal phase region ($0.15 \leq x \leq 0.30$). With increasing BST content, the BNT-BST ceramics undergo a ferroelectric to relaxor state transformation accompanied by a gradually decrease of T_m from ~ 250 °C to near room temperature. For BNT-BST ceramics with relaxor ferroelectric state ($x \geq 0.15$), both the P_r and E_c gradually reduce with increasing BST content due to an enhanced nonpolar tetragonal (*P*4*bm*) and/or Cubic ($Pm\bar{3}m$) structure. The relaxor BNT-BST ceramics possess both high peak dielectric constant ($\varepsilon_r > 6000$ at T_m) and saturated polarization ($P_s \sim 30$ μC/cm^2), in addition to tunable remnant polarization P_r, which is suitable for application of good capacitor candidate materials.

Acknowledgements This work was financially supported by National Natural Science Foundation of China (51767010), Science & Technology Key Research Project of Jiangxi Provincial Education Department (GJJ170760) and Graduate Student Innovation Fund of Jiangxi Province (YC2018-S295).

References

1. W.J. Sarjeant, J. Zirnheld, F.W. MacDougall, J.S. Bowers, N. Clark, I.W. Clelland, R.A. Price, M. Hudis, I. Kohlberg, G. McDuff, I. McNab, S.G. Parler, Jr.J. Prymak, Capacitors—past, present, and future, Handb. Low High Dielectr. Constant. Mater. Appl. **2**, 423–491 (1999)
2. C.A. Randall, H. Ogihara, J.R. Kim, G.Y. Yang, C.S. Stringer, S. Trolier-McKinstry, Proceedings of the IEEE Pulsed Power Conference, p346 (2009)
3. M.E. Lines, A.M. Glass, *Principles and applications of ferroelectrics and related materials* (Oxford University Press, New York, 2004), pp. 241–255
4. L.E. Cross, Ferroelectrics **76**, 241–267 (1987)
5. R.A. Cowley, S.N. Gvasaliya, S.G. Lushnikov, B. Roessli, G.M. Rotaru, Adv. Phys. **60**, 229–327 (2011)
6. K. Uchino, Chap. 3 - Relaxor Ferroelectric-Based Ceramics, Advanced Piezoelectric Materials (2nd edn.) p. 127–153 (2017)
7. F. Li, S. Zhang, T. Yang, Z. Xu, N. Zhang, G. Liu, J. Wang, J. Wang, Z. Cheng, Z. Ye, J. Luo, T.R. Shrout, L.Q. Chen, Nat. Commun. **7**, 13807 (2016)
8. W. Jia, Y. Hou, M. Zheng, Y. Xu, M. Zhu, K. Yang, H. Cheng, S. Sun, J. Xing, IET Nanodielectr. **1**, 3–16 (2018)
9. J. Hao, W. Li, J. Zhai, H. Chen, Mater. Sci. Eng. R **135**, 1–57 (2019)
10. W.P. Cao, W.L. Li, X.F. Dai, T.D. Zhang, J. Sheng, Y.F. Hou, W.D. Fei, J. Eur. Ceram. Soc. **36**, 593–600 (2016)
11. Q. Xu, Z. Song, W. Tang, H. Hao, L. Zhang, M. Appiah, M. Cao, Z. Yao, Z. He, H. Liu, J. Am. Ceram. Soc. **98**, 3119–3126 (2015)
12. G.A. Smolenskii, V.A. Isupov, A.I. Agranovskaya, N.N. Krainik, Sov. Phys. Solid State **2**, 2651–2654 (1961)
13. C.S. Tu, I.G. Siny, V.H. Schmidt, Phys. Rev. B **49**, 11550–11559 (1994)
14. S.R. Kanuru, K. Baskar, R. Dhanasekaran, Ceram. Int. **42**, 6054–6064 (2016)
15. A. Sasaki, T. Chiba, Y. Mamiya, E. Otsuki, Jpn. J. Appl. Phys. **38**, 5564–5567 (1999)
16. J. Wang, H. Fan, B. Hu, H. Jiang, J. Mater. Sci.: Mater. Electron. (2018). https://doi.org/10.1007/s10854-018-0522-y
17. W. Ma, Y. Zhu, M.A. Marwat, P. Fan, B. Xie, D. Salamon, Z.G. Ye, H. Zhang, J. Mater. Chem. C **7**, 281–288 (2019)
18. M. Acosta, J. Zang, W. Jo, J. Rödel, J. Eur. Ceram. Soc. **32**, 4327–4334 (2012)
19. R. Dittmer, E.M. Anton, W. Jo, H. Simons, J.E. Daniels, M. Hoffman, J. Pokorny, I.M. Reaney, J. Rödel, J. Am. Ceram. Soc. **95**, 3519–3524 (2012)
20. M. Xiao, H. Sun, Y. Wei, L. Li, P. Zhang, J. Mater. Sci.: Mater. Electron. **29**, 17689–17694 (2018)
21. Y. Wang, Z.Y. Shen, Y.M. Li, Z.M. Wang, W.Q. Luo, Y. Hong, Ceram. Int. **41**, 8252–8256 (2015)
22. Z.Y. Shen, Y.Y. Yu, Y. Wang, L. Zhang, W.Q. Luo, Z.M. Wang, Y.M. Li, J. Mater. Sci.: Mater. Electron. **29**, 1093–1097 (2018)
23. M. Chen, Q. Xu, B.H. Kim, B.K. Ahn, J.H. Ko, W.J. Kang, O.J. Nam, J. Eur. Ceram. Soc. **28**, 843–849 (2008)
24. K. Wang, A. Hussain, W. Jo, J. Rödel, J. Am. Ceram. Soc. **95**, 2241–2247 (2012)
25. V.V. Shvartsman, D.C. Lupascu, J. Am. Ceram. Soc. **95**, 1–26 (2012)